Form Approved
OMB No. 0704-0188

1. AGENCY USE ONLY (Leave blank) | 2. REPORT DATE: Feb 23 1994 | 3. REPORT TYPE AND DATES COVERED: Reprint

4. TITLE AND SUBTITLE

OH $A\,^2\Sigma^+ \rightarrow X\,^2\Pi$ chemiluminescence measurements of N_2^+, $Ar^+ + H_2O$ hydrogen-atom-transfer reactions at suprathermal energies

5. FUNDING NUMBERS

PE 61102F
PR 2303
TA G2
WU 01

6. AUTHOR(S)

James A. Gardner*, Rainer A. Dressler, Richard H. Salter, Edmond Murad

7. PERFORMING ORGANIZATION NAME(S) AND ADDRESS(ES)

Phillips Lab/WSSI
29 Randolph Road
Hanscom AFB, MA 01731-3010

8. PERFORMING ORGANIZATION REPORT NUMBER

PL-TR-94-2037

9. SPONSORING/MONITORING AGENCY NAME(S) AND ADDRESS(ES)

10. SPONSORING/MONITORING AGENCY REPORT NUMBER

11. SUPPLEMENTARY NOTES *PhotoMetrics, Inc.

Reprinted from J. Chem. Phys. 97 (4) 15 August 1992

12a. DISTRIBUTION/AVAILABILITY STATEMENT

Approved for public release; Distribution unlimited

13. ABSTRACT (Maximum 200 words)

Chemiluminescence attributable to OH $A\,^2\Sigma^+ \rightarrow X\,^2\Pi$ emission is observed in hydrogen-atom transfer reactions of N_2^+ and Ar^+ with H_2O. High-resolution OH $A \rightarrow X$ spectra [0.5 nm full width at half maximum (FWHM)] are presented as a function of collision energy in the range $E_{c.m.}$ = 5–20 eV. The spectra clearly show an increase in rotational broadening with collision energy. To reasonably fit the spectral data, simulations require contributions from two Boltzmann distributions with different rotational temperatures. It is proposed that the OH A state is formed via two channels. In the dominant channel, A state OH is formed in both $v' = 0$ and $v' = 1$, with a collision energy-dependent rotational temperature ranging from 1000 K at $E_{c.m.}$ = 6 eV to 3400 K at $E_{c.m.}$ = 19 eV. The rotationally excited products are proposed to be formed in a two-step reaction involving charge transfer, followed by the transfer of a proton to the "primary" species. The second channel is characterized by formation of A state OH primarily in the $v' = 0$ vibrational level with a rotational temperature of 300 K. Comparison of low-resolution (4 nm FWHM) OH $A \rightarrow X$ and H_2O^+ $\tilde{A}\,^2A_1 \rightarrow \tilde{X}\,^2B_1$ emissions provides an estimate for the OH A state cross sections of $\sigma < 0.3 \times 10^{-16}$ cm^2 for $N_2^+ + H_2O$ at $E_{c.m.}$ between 6 and 20 eV, representing less than 10% of the hydrogen atom pickup channel at these energies. For $Ar^+ + H_2O$ at $E_{c.m.}$ between 11 and 32 eV, the estimated OH A state cross section is $\sigma < 0.5$ Å^2, which may represent all of the hydrogen atom pickup channel at the higher energies.

14. SUBJECT TERMS

Ion-molecule interactions, Hydrogen-atom transfer, Chemiluminescence, Cross section, Water

15. NUMBER OF PAGES: 8

16. PRICE CODE

17. SECURITY CLASSIFICATION OF REPORT	18. SECURITY CLASSIFICATION OF THIS PAGE	19. SECURITY CLASSIFICATION OF ABSTRACT	20. LIMITATION OF ABSTRACT
UNCLASSIFIED	UNCLASSIFIED	UNCLASSIFIED	SAR

OH $A\,^2\Sigma^+ \rightarrow X\,^2\Pi$ chemiluminescence measurements of N_2^+, $Ar^+ + H_2O$ hydrogen-atom-transfer reactions at suprathermal energies

James A. Gardner,[a] Rainer A. Dressler, Richard H. Salter, and Edmond Murad
Phillips Laboratory,[b] Spacecraft Interactions Branch, PL/WSSI,
Hanscom Air Force Base, Massachusetts 01731-5000

(Received 8 April 1992; accepted 8 May 1992)

Chemiluminescence attributable to OH $A\,^2\Sigma^+ \rightarrow X\,^2\Pi$ emission is observed in hydrogen-atom transfer reactions of N_2^+ and Ar^+ with H_2O. High-resolution OH $A \rightarrow X$ spectra [0.5 nm full width at half maximum (FWHM)] are presented as a function of collision energy in the range $E_{c.m.} = 5$–20 eV. The spectra clearly show an increase in rotational broadening with collision energy. To reasonably fit the spectral data, simulations require contributions from two Boltzmann distributions with different rotational temperatures. It is proposed that the OH A state is formed via two channels. In the dominant channel, A state OH is formed in both $v' = 0$ and $v' = 1$, with a collision energy-dependent rotational temperature ranging from 1000 K at $E_{c.m.} = 6$ eV to 3400 K at $E_{c.m.} = 19$ eV. The rotationally excited products are proposed to be formed in a two-step reaction involving charge transfer, followed by the transfer of a proton to the "primary" species. The second channel is characterized by formation of A state OH primarily in the $v' = 0$ vibrational level with a rotational temperature of 300 K. Comparison of low-resolution (4 nm FWHM) OH $A \rightarrow X$ and H_2O^+ $\tilde{A}\,^2A_1 \rightarrow \tilde{X}\,^2B_1$ emissions provides an estimate for the OH A state cross sections of $\sigma < 0.?\times 10^{-16}$ cm^2 for $N_2^+ + H_2O$ at $E_{c.m.}$ between 6 and 20 eV, representing less than 10% of the hydrogen atom pickup channel at these energies. For $Ar^+ + H_2O$ at $E_{c.m.}$ between 11 and 32 eV, the estimated OH A state cross section is $\sigma < 0.5$ Å^2, which may represent all of the hydrogen atom pickup channel at the higher energies.

I. INTRODUCTION

Gas phase ion-molecule reactions proceed primarily through a direct mechanism[1] at suprathermal energies (i.e., at center-of-mass reaction energies, $E_{c.m.}$, from 1 to 50 eV). Exothermic direct processes exhibit large cross sections if they are efficient at large impact parameters. Little momentum is transferred in such collisions, thus large cross sections are only observed for the transfer of low mass particles (e.g., e^-, H, H^+, H^-), while most of the reaction exothermicity is channeled into internal excitation of the products.[2,3] Electron transfer is the simplest direct process in ion-molecule collisions. Exothermic charge-transfer processes do not require a significant momentum transfer; therefore, a long-range electron hop is possible and large suprathermal charge-transfer cross sections are frequently observed.[2,4–10] It has been postulated that the magnitude of the state-to-state charge-transfer cross section is a function both of the Franck–Condon overlap between the reactant and product vibronic wave functions, and of the energy gap between the reactant and product energy levels.[11–15] Recently, we have reported[16,17] intense luminescence from the charge–transfer systems:

$$N_2^+ + H_2O \rightarrow N_2 + H_2O^+ + 2.96\ \text{eV} \quad (1)$$

and

$$Ar^+ + H_2O \rightarrow Ar + H_2O^+ + 3.14\ \text{eV}. \quad (2)$$

The analysis of the luminescence spectra shows that large suprathermal cross sections result from population of highly vibrationally excited H_2O^+ $\tilde{A}\,^2A_1$ levels that are near resonant with the reactant energy level, as predicted by the Franck–Condon and energy resonance arguments.

The simplest gas phase ion-molecule chemical reactions are those involving the transfer of a hydrogen atom or ion. Suprathermal hydrogen transfer reactions have been postulated to occur either directly[2,18] or through a nonadiabatic channel involving a charge-transfer intermediate species.[19,20] The spectator stripping kinematic model, which is a specialized case of the pairwise energy model,[21] considers the reaction as occurring solely between the primary ion and the hydrogen atom being stripped, and the remainder of the target molecule is termed the spectator of the overall reaction. The nonadiabatic transfer model invokes a transition from the primary reactant surface to the charge–transfer surface as the first step in the hydrogen atom transfer. In the $Ar^+ + H_2 \rightarrow ArH^+ + H$ system, for example, proton transfer on the $Ar + H_2^+$ surface is the most likely pathway for the overall reaction.[19]

The suprathermal reactions of N_2^+ and Ar^+ with H_2O each exhibit a hydrogen atom abstraction channel:

$$N_2^+ + H_2O \rightarrow N_2H^+ + OH + 1.9\ \text{eV} \quad (3)$$

and

$$Ar^+ + H_2O \rightarrow ArH^+ + OH + 0.9\ \text{eV}. \quad (4)$$

Reactions (3) and (4) account for approximately 5–10 % of the total $N_2^+ + H_2O$ and $Ar^+ + H_2O$ reaction cross sections.[2,22,23] Product ion kinetic-energy measurements have been previously reported for reaction (4) (Ref. 23) and for

[a] PhotoMetrics, Inc.
[b] Formerly the Geophysics Laboratory.

 0021-9606/92/162473-08$06.00

the deuterated analog of reaction (3) (Ref. 2). In those cases, the product ion translational energy is in good agreement with the pairwise energy prediction.

Observation of ionic species is sufficient to provide ion-neutral reaction cross sections; however, the spectroscopy of chemiluminescent ionic and neutral products can provide additional information regarding the reaction dynamics.[24,25] The $N_2^+ + H_2O$ and $Ar^+ + H_2O$ collision systems are the first reported systems that produce optical emissions in both charge transfer and chemical exchange channels. Reactions (3) and (4) exhibit chemiluminescence that is attributable to the neutral product OH $A\,^2\Sigma^+ \rightarrow X\,^2\Pi$ transition. The formation of A state OH is endothermic by 2.1 and 3.1 eV in reactions (3) and (4), respectively.[26] Thus, the chemiluminescent OH products are formed in smaller impact parameter collisions than those resulting in luminescent charge-transfer products.

We report here a study of the OH $A\,^2\Sigma^+ \rightarrow X\,^2\Pi$ chemiluminescence in reactions (3) and (4), measured over the collision energy range of $E_{c.m.} = 5$–20 eV. High-resolution spectra [0.5 nm full width at half maximum (FWHM)] show contributions from the (0,0), (1,0), and (1,1) vibrational bands of the OH $A \rightarrow X$ transition. Rotational broadening of these bands is observed as the collision energy is increased. Simulations have been performed to determine the nascent rotational population of the OH A state product. The experimental and simulation techniques are described in Sec. II. Spectral data and the simulation results are presented in Sec. III. An estimate of the OH A state formation cross section is presented in Sec. IV, along with a discussion of the dynamics involved in production of the excited OH.

II. EXPERIMENT

The chemiluminescence measurement apparatus consists of an ion beam–static gas collision cell in a double mass spectrometer/emission detection system that has been described in detail previously.[17,27] Briefly, an ion beam is formed in a dc plasma discharge ion source, accelerated into and mass selected by a Wien velocity filter, decelerated in two stages to the desired collision energy, and passed through a 1.9 cm path length cell containing the target gas (H_2O) maintained at 1.5 mTorr. The mean free path is approximately 2 orders of magnitude longer than the cell dimension, thus secondary collisions that could change the A state OH rotational and/or vibrational population[28,29] are insignificant here.

To measure the primary ion energy, retardation potential scans are performed using a set of fine grids following the collision chamber. A quadrupole mass filter provides ion identification. The primary ion beam current impinging on a grid following the collision chamber is measured by an electrometer and recorded on a chart recorder. A vacuum-sealed fiberoptic bundle guides emitted light from the collision chamber to an external spectrograph and optical multichannel analyzer (OMA, Princeton Instruments) that is equipped with an S-20 photocathode and an intensified photodiode array (730 active diodes). The OMA data consists of signal and background exposures, each lasting 30 min, for which the ion beam alternately passes through the target gas cell or is deflected prior to the cell. The apparatus produces no optical background signal; however, the background scans are required to properly account for the diode noise in the OMA collector. For the data presented here, a final spectrum is the sum of 2 to 125 such (signal-background) scans. A mercury lamp is used to calibrate the wavelength scale. Using a deuterium lamp, the detector spectral response is found to be constant over the wavelength range of interest to high-resolution measurements in this study, i.e., 280–320 nm. Low-resolution measurements are also presented here for which the OMA spectral response is measured using a tungsten halogen lamp with a color temperature of 3200 K.[17]

Simulations of the spectra are performed to determine the rotational temperature of the OH A state products. For the simulations, it is assumed that the A state OH has a Boltzmann rotational population with a characteristic temperature. Gaussian profiles are used for the simulation lines, with the widths set to 0.55 nm for the high-resolution simulations. The transition line intensities are taken from Dieke and Crosswhite,[30] and the line positions are calculated from energies tabulated therein. Good fits to the data are obtained with the rotational transition probabilities scaled as 1:0.26:0.47 for[31] $(v',v'') = (0,0):(1,0):(1,1)$, in good agreement with the transition probability ratios reported by Chidsey and Crosley.[32]

The spectroscopy of the OH $A\,^2\Sigma^+ \rightarrow X\,^2\Pi$ transition is well known and has been documented by Dieke and Crosswhite.[30] Briefly, this transition is intermediate between Hund's case (a) and case (b), with slow rotation levels closest to case (a), and fast rotation levels closest to case (b). The selection rule for the $A \rightarrow X$ transition is $\Delta J = 0 \pm 1$ where J, the total angular momentum quantum number, is equal to $K + \frac{1}{2}$ and K is the total angular momentum quantum number apart from electron spin. For Hund's case (b), there is a further selection rule: $\Delta K = 0 \pm 1$. There are twelve possible branches: the six main branches ($\Delta J = 0$) are P_1, P_2, Q_1, Q_2, R_1, and R_2; the six satellite branches ($\Delta J = \pm 1$) are O_{12}, P_{12}, Q_{21}, Q_{12}, R_{21}, and S_{21}. Here O, P, Q, R, and S refer to the transitions $\Delta K = 2$, 1, 0, -1, and -2, respectively. The subscripted indices 1 and 2 refer, respectively, to the states $J = K + \frac{1}{2}$ and $J = K - \frac{1}{2}$; and where two subscripts are shown, the first refers to the upper (A) state value and the second refers to the lower (X) state value. For comparison, at 3000 K the strongest lines in the main branches are 5 to 10 times more intense than the strongest lines in the satellite branches.[30] The radiative lifetimes of the low rotational levels in the OH A state have been reported to be $\tau = 693 \pm 30$ ns for $v = 0$ and $\tau = 736 \pm 39$ ns for $v = 1$.[33]

III. RESULTS

A. Chemiluminescence data

Luminescence measurements for $N_2^+ + H_2O$ and $Ar^+ + H_2O$ collisions reveal both OH $A \rightarrow X$ and H_2O^+ $\tilde{A}\,^2A_1 \rightarrow \tilde{X}\,^2B_1$ emissions.[16,17] Low resolution (4 nm FWHM) spectra are shown for these two systems as a function of collision energy in Figs. 1 and 2, respectively. The relevant emission spectral regions are marked in both fig-

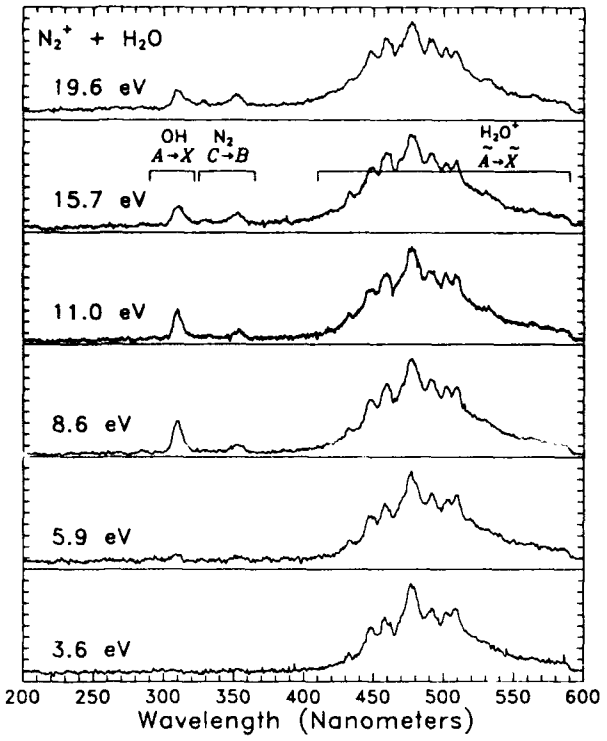

FIG. 1. Low-resolution (4 nm FWHM) chemiluminescence measurements at several center-of-mass energies for $N_2^+ + H_2O$ reactions. The spectral ranges of significant OH, N_2, and H_2O^+ emissions are labeled.

ures. The signal dropouts observed at 210 and 590 nm indicate the OMA active detection range for these measurements. For both systems, the H_2O^+ emissions are the dominant signal and are found at all energies reported here. The OH emissions exhibit an energy dependence, with an onset near 6 eV for $N_2^+ + H_2O$ and near 11 eV for $Ar^+ + H_2O$. This behavior is qualitatively consistent with the OH A state formation being an endothermic process and the H_2O^+ $\tilde{A}$ state formation being an exothermic process. At the higher energies in Fig. 1, emissions are also observed in the N_2 second positive system,[34] which is excited by inelastic charge transfer collisions. In all figures presented here, the data and simulations are normalized to their highest peak.

A 1 nm (FWHM) resolution emission measurement for $Ar^+ + H_2O$ at $E_{c.m.} = 16$ eV is shown in Fig. 3. The arrows show the bandheads for (v',v'') transitions with $v' = 0 - 3$ in the wavelength range of interest. The horizontal bars show the range from each band head to the corresponding $P_2(N'' = 15)$ line, which is arbitrarily chosen to provide a wavelength range that includes most of the band's emissions. The dashed line represents the zero signal level. The OH emissions attributable to the (0,0), (1,0), and (1,1) vibrational bands are readily identified in Fig. 3. As resolution and the signal-to-noise ratio are increased, no emissions are found to be attributable to $v' = 2$ or 3 bands. The OH A state $v' = 2$ level has been reported to fully predissociate, with decay lifetimes of < 200 ns.[33,35] A recent study of the predissociation in the $v' = 3$ level[35] calculates lifetimes for this vibrational level to be on the order of 100 ps. Thus, no emissions are expected even if these upper levels are initially populated.

High-resolution (0.5 nm FWHM) measurements have been performed at several collision energies for reactions (3) and (4), and are displayed in Figs. 4 and 5. Rotational broadening clearly increases as the collision energy increases. Above $E_{c.m.} = 20$ eV, minor N_2 (second positive system)[34] emissions are also observed at 313–316 nm in the $N_2^+ + H_2O$ case. These N_2 emissions are, however, below the noise level for the data presented here.

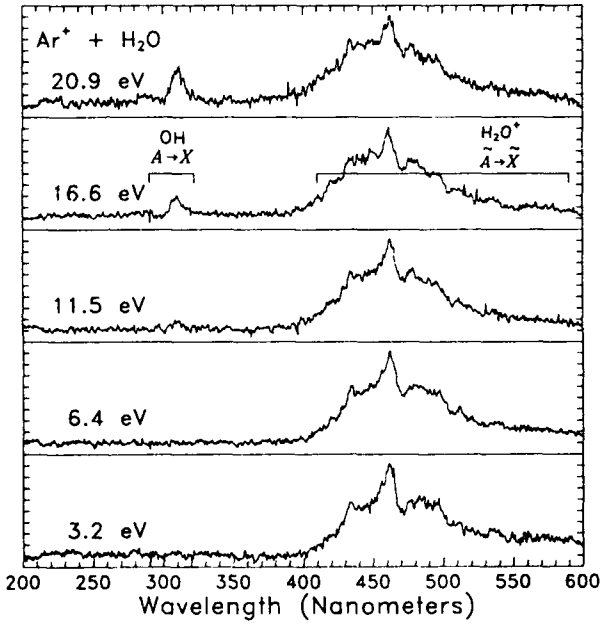

FIG. 2. Low-resolution (4 nm FWHM) chemiluminescence measurements at several center-of-mass energies for $Ar^+ + H_2O$ reactions. The spectral ranges of significant OH and H_2O^+ emissions are labeled.

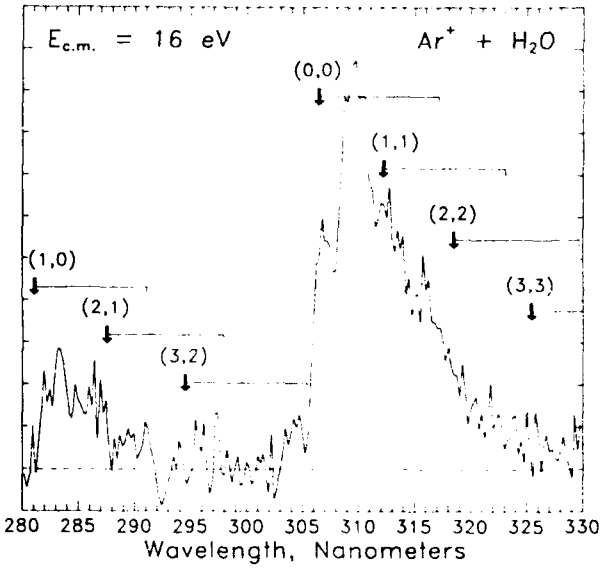

FIG. 3. Medium-resolution (1 nm FWHM) chemiluminescence spectrum for $Ar^+ + H_2O$ at $E_{c.m.} = 16$ eV. Arrows show the bandheads for (v',v'') transitions with $v' \leq 3$ in the wavelength range of interest. Horizontal bars show range of band up to $P_2(15)$.

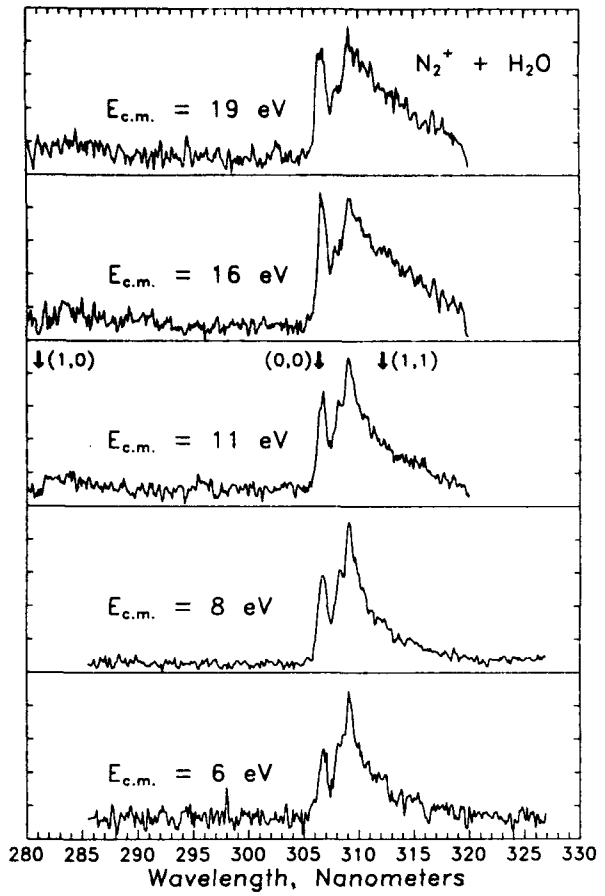

FIG. 4. High-resolution (0.5 nm FWHM) chemiluminescence measurements at several center-of-mass energies for $N_2^+ + H_2O$ reactions. The bandheads for the (0,0), (1,0), and (1,1) transitions are shown.

B. Simulation results

Within each vibrational band of the OH $A \rightarrow X$ transition, the dominant rotational branches are the P_1, P_2, Q_1, Q_2, R_1, and R_2 branches. Rotational line positions in these branches are shown for the (0,0) band in Fig. 6, where the labels indicate the N'' levels. For comparison, the high-resolution emission data for $N_2^+ + H_2O$ at $E_{c.m.} = 6$ eV is also shown in Fig. 6. The dominant features in the data are the (0,0) R branches at 306–307 nm, the (0,0) Q-branch peaks from 308 to 310 nm, and the (0,0) P branches broadening above 309 nm. Additionally, the (1,1) R branches peak at 312–313 nm; the (1,1) Q branches peak at 313–315 nm, and the (1,1) P-branches broadening contribution is important above 314 nm. Simulation parameters are adjusted to provide the best visual fit to these features and to match the relative intensities of the (1,v'') bands.

A good fit to the data is not found when a single rotational temperature is used in the simulations. However, as shown in Fig. 7, the combination of two T_{rot} simulations provides a good fit to the emission data. The individual simulations for $T_{rot} = 300$ K ($v' = 0$) and $T_{rot} = 3400$ K ($v' = 0,1$) are shown (solid lines) superimposed on the high-resolution emission data (dashed lines) for $Ar^+ + H_2O$ at $E_{c.m.} = 19$ eV. Clearly, neither simulation by itself provides a good fit to this data. Furthermore, increasing T_{rot} in 100 K increments between 300 and 3400 K does not provide any single simulation with a reasonable fit. As also shown in Fig. 7, however, the combination of the two simulations for $T_{rot} = 300$ K and 3400 K does reproduce the experimental data well. In this combination, the weighting of the two components is 1:4.0 for the 300:3400 K simulations.

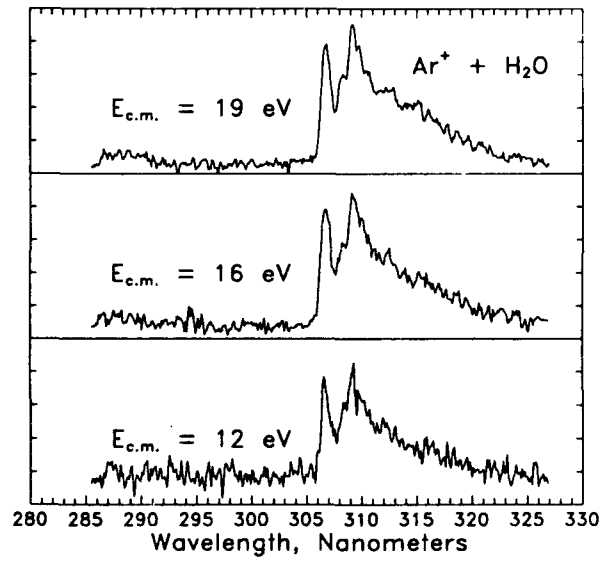

FIG. 5. High-resolution (0.5 nm FWHM) chemiluminescence measurements at several center-of-mass energies for $Ar^+ + H_2O$ reactions.

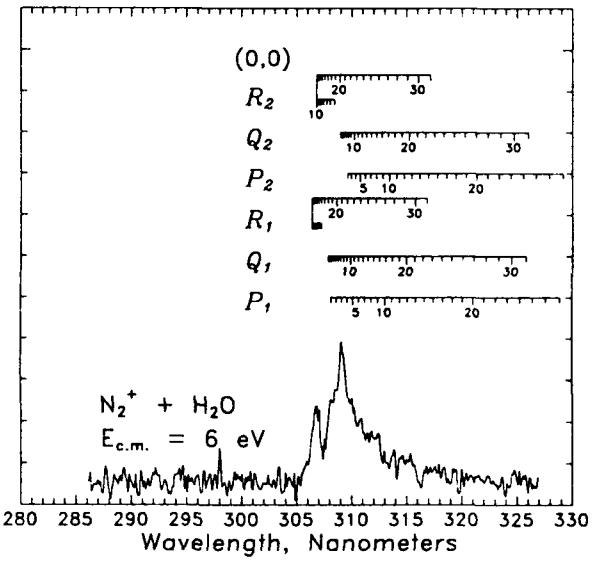

FIG. 6. Line positions for the main rotational branches in the OH $A \rightarrow X$ (0,0) vibrational band. Shown for comparison is the high-resolution emission data for $N_2^+ + H_2O$ at $E_{c.m.} = 6$ eV.

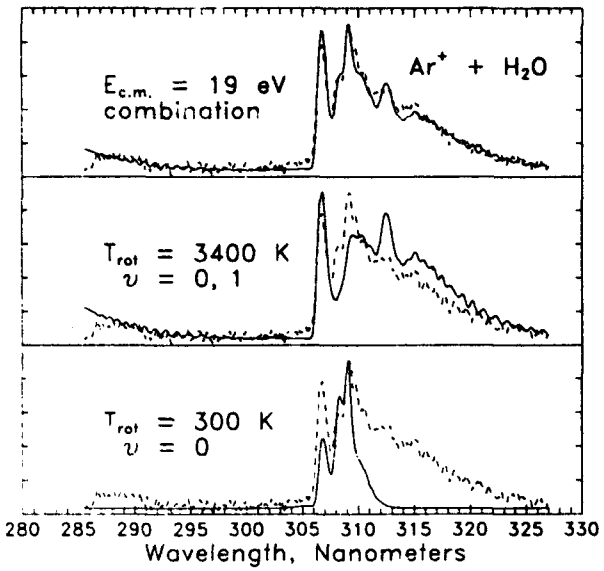

FIG. 7. High-resolution spectral data (dashed lines) for $Ar^+ + H_2O$ at $E_{c.m.} = 19$ eV with simulations (solid lines) $T_{rot} = 300$ K, $v' = 0$; $T_{rot} = 3400$ K, $v' = 0,1$; and the combination of the two simulations with a 1:4.0 weighting for the 300:3400 K components.

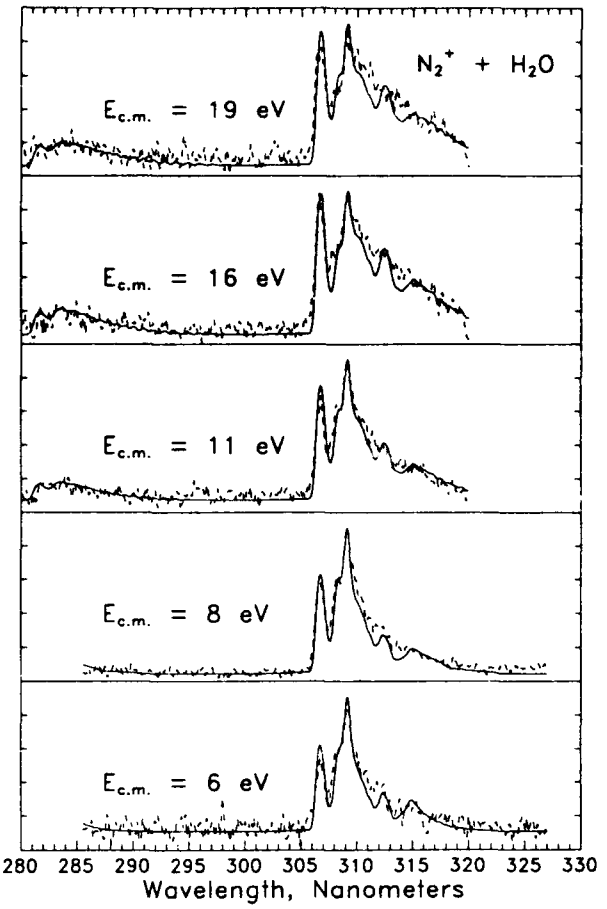

FIG. 8. Simulations (solid lines) for the $N_2^+ + H_2O$ spectral data (dashed lines).

Likewise, the remaining high-resolution data has been simulated. The best fits are shown (solid lines) superimposed on the experimental data (dashed lines) for $N_2^+ + H_2O$ and $Ar^+ + H_2O$ in Figs. 8 and 9, respectively. In all cases, the best fit is obtained by using a low $T_{rot} = 300$ K component, with $v' = 0$ populated, along with a high T_{rot} component, in which both $v' = 0$ and $v' = 1$ are populated. In all high T_{rot} cases, the $v' = 1$:$v' = 0$ population ratio is 0.75:1. For a Boltzmann population, this ratio corresponds to a vibrational temperature of $T_{vib} \approx 16\,000$ K ($E_{vib} = 1.35$ eV), and would also indicate that approximately 66% of the A state OH is produced in vibrational levels above $v' = 1$. As mentioned earlier, no emissions are observed from $v' > 2$ levels, because these levels either are not populated or are fully predissociated. In other systems, non-Boltzmann vibrational populations have been observed;[24] however, a definitive statement on the population is not possible here. In the $T_{rot} = 300$ K case, population of the $v' = 1$ level cannot be ruled out; however, the agreement between the simulations and experimental data is significantly degraded when the $T_{rot} = 300$ K $v' = 1$ level is set to provide 10% of the total $v' = 1$ contribution (i.e., $v' = 1$:$v' = 0$ equals 0.075:1). This level corresponds to a Boltzmann population of $T_{vib} \approx 1800$ K ($E_{vib} = 0.15$ eV), with less than 0.6% of the population above $v' = 1$, and represents an extreme upper limit to the $v' = 1$ population in the $T_{rot} = 300$ K case. Because the signal that this level contributes to the overall simulation is negligible, the $v' = 1$ population is set to zero in the $T_{rot} = 300$ K component of all simulations.

The primary simulation variables are the value of the high T_{rot} and the relative weighting of the two T_{rot} simulation components. These variables are summarized in Table I along with the average rotational energies, E_{rot}, for the high T_{rot} distributions. The high T_{rot} values for the simulations are also plotted as a function of collision energy in Fig. 10, where a monotonic increase in T_{rot} with increasing collision energy is visible. While performing the simulations, the rota-

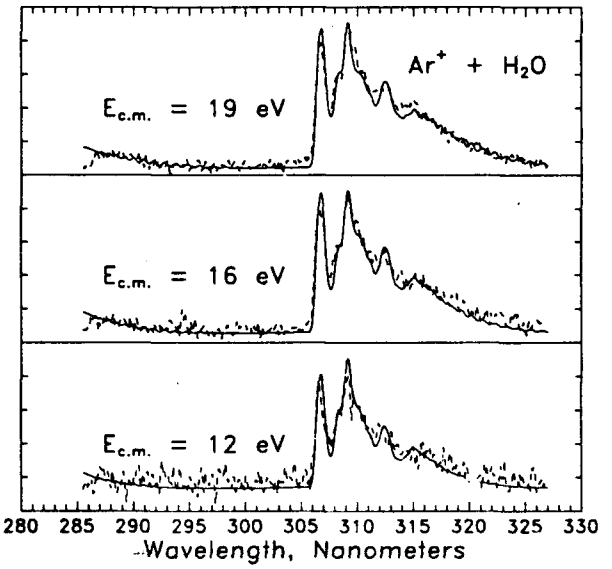

FIG. 9. Simulations (solid lines) for the $Ar^+ + H_2O$ spectral data (dashed lines).

TABLE I. Parameters for best fits in simulations of spectral data along with the rotational energy, E_{rot}, corresponding to the high rotational temperature, T_{rot}, case.

	$E_{c.m.}$ (eV)	High T_{rot}, (K)	E_{rot} (eV)	Low:High T_{rot} weights
$N_2^+ + H_2O$	6	1000	0.08	1:1.8
	8	1600	0.13	1:1.2
	11	2300	0.19	1:2.2
	16	2600	0.22	1:4.4
	19	3000	0.25	1:3.8
$Ar^+ + H_2O$	12	2000	0.17	1:3.1
	16	2600	0.22	1:4.4
	19	3400	0.29	1:4.0

tional temperatures of the $v' = 0$ and $v' = 1$ levels in the high T_{rot} component were first independently varied, but found to be equal. A similar occurrence of matching T_{rot} in different v' levels has been reported by Kusunoki and Ottinger[36] for measurements of $CH^+(CD^+)$ chemiluminescence in $C^+ + H_2(D_2)$ reactions.

Predissociation of the A state above $N' = 23$ in the $v' = 0$ band, and above $N' = 14$ in the $v' = 1$ bands, shortens the radiative lifetimes of these levels.[33,37] Simulations have been performed to consider the possibility that the predissociation may entirely quench emission from these levels, thereby affecting the spectra. In Fig. 11, the data for $Ar^+ + H_2O$ at $E_{c.m.} = 19$ eV is shown with simulations that alternately include (lower plot) and disregard (upper plot) total quenching. To include the quenching, the calculation is truncated at the predissociation limits. This has no effect on the $T_{rot} = 300$ K component of the simulation, because the rotational population falls to essentially zero by $N' = 10$.

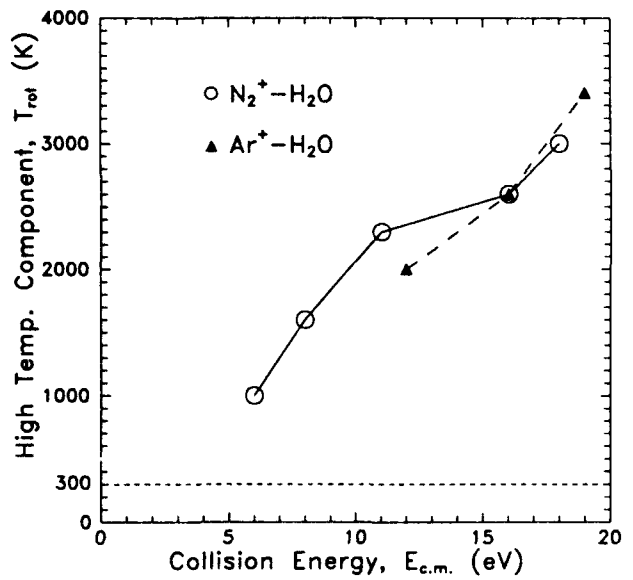

FIG. 10. Collision energy dependence of the high T_{rot} component in the simulations.

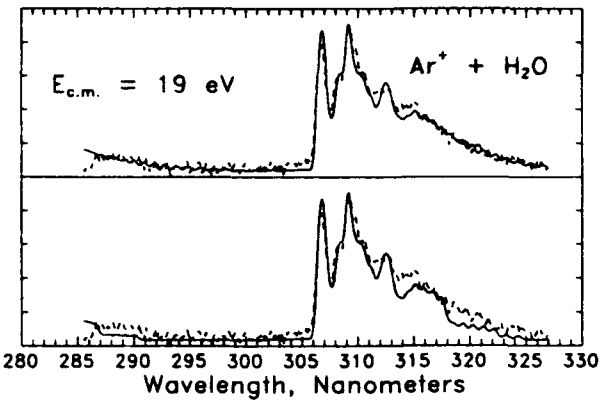

FIG. 11. Simulations for $Ar^+ + H_2O$ emissions at $E_{c.m.} = 19$ eV, alternately including (lower plot) and disregarding (upper plot) the possible quenching of emissions due to predissociation above $N' = 23$ in $v' = 0$, and above $N' = 14$ in $v' = 1$.

For $T_{rot} = 3400$ K, however, rotational levels up to $N' = 30$ are populated, and the inclusion of such quenching causes a significant change in the simulation result, particularly around 286–291 nm and 317–327 nm. The simulations that do not include predissociative emission quenching exhibit better agreement with the data. Thus, predissociation has no significant affect on the spectra at the present experimental conditions (i.e., spectral resolution) and is not included in the final simulations.

IV. DISCUSSION

A. OH *A* state formation cross sections

The OH A state formation cross section can be estimated using the low resolution measurements in Figs. 1 and 2. The total OH and H_2O^+ emission intensities have been integrated, accounting for the OMA spectral response. An estimate of the OH A state formation cross section is given by the ratio of the OH:H_2O^+ emission intensities multiplied by the appropriate charge transfer cross sections. This assumes that (i) the collection efficiency is the same for both types of emissions, (ii) all H_2O^+ formed in reactions (1) and (2) is produced in the $\tilde{A}$ state and therefore emits, and (iii) all A state OH formed in reactions (3) and (4) emits. The H_2O^+ $\tilde{A} \rightarrow \tilde{X}$ and OH $A \rightarrow X$ states have similar radiative lifetimes ($\tau = 800$ ns for H_2O^+ $\tilde{A} \rightarrow \tilde{X}$ and 700 ns for OH $A \rightarrow X$).[33,38] Past studies[2,23] have shown that H_2O^+ produced in reactions (1) and (2) is formed with very little momentum transfer; i.e., the H_2O^+ has near-thermal translational energy in the laboratory frame. Time-of-flight measurements on the ionic products of the deuterated analogs of reactions (3) and (4) indicate a spectator stripping type mechanism, in which the OH(OD) co-product experiences no significant increase in velocity during the collision and is therefore also formed with near-thermal translational energy. With similar radiative lifetimes and translational energy distributions for the H_2O^+ and OH, their emissions will have similar spatial distributions. Thus, the first assumption is justified.

The analysis of the $H_2O^+ \tilde{A} \rightarrow \tilde{X}$ emissions in reactions (1) and (2) (Ref. 17) shows that the population of $H_2O^+ \tilde{A}$ state levels, following charge transfer, is strongly related to H_2O ionization Franck–Condon factors. It is therefore assumed that the majority of the H_2O^+ is produced in the $\tilde{A}$ state. The luminescence measurements cannot detect any H_2O^+ that may be directly formed in the $\tilde{X}$ state; therefore, the derived OH A state formation cross sections are upper limits to the actual cross sections. Because A state OH that may be formed in vibrational levels $v' \geq 2$ can predissociate, the derived cross sections may also underestimate the total A state formation cross section. They do, however, serve as a reasonable estimate (i.e., within about a factor of 2) for this cross section.

The estimates calculated for the A state OH formation cross sections are plotted as a function of collision energy in Fig. 12 for both reactions (3) and (4). Above $E_{c.m.} = 5$ eV, comparison of these estimated cross sections with recent N_2H^+ cross-section measurements[39] show the A state formation to account for approximately 10% of the reaction (3) cross section and, therefore, less than 1% of the total reaction cross section for $N_2^+ + H_2O$ collisions. The total cross section for reaction (4) is significantly smaller than that of reaction (3) above $E_{c.m.} = 5$ eV.[39] Above 15 eV, the OH A state formation may account for all of the reaction (4) cross section. At $E_{c.m.} > 30$ eV, hydrogen atom Balmer series emissions are observed in the $Ar^+ + H_2O$ system.[17] The increase in OH emissions at 32 eV may result from dissociative processes similar to those forming the excited hydrogen atoms. The hydrogen atom emissions are only observed at much higher collision energies in the $N_2^+ + H_2O$ system.[17]

As seen in Fig. 12, the estimated value for the OH A state formation cross section is less than 0.5 Å.[2] In its simplest form, the reaction cross section, σ, can be written as

$$\sigma = \tilde{P}\pi\tilde{R}^2,$$

where $\tilde{P}$ is the average probability for a reaction to occur and $\tilde{R}$ is the intermolecular distance along the scattering trajectory at which the particular transfer is most probable. For $\sigma = 0.5$ Å^2, a large impact parameter collision ($\tilde{R} > 3$ Å) would have an extremely small probability ($\tilde{P} < 0.02$), and even a very small impact parameter collision would have a relatively low probability of reaction (for $\tilde{R} = 1$ Å, $\tilde{P} = 0.16$). Formation of A state OH may therefore proceed as an extremely inefficient process in large impact parameter collisions, or as a moderately efficient process at smaller impact parameters. The translational-to-internal energy conversion that is required to overcome the endothermicity in forming A state OH is consistent with a small impact parameter collision.

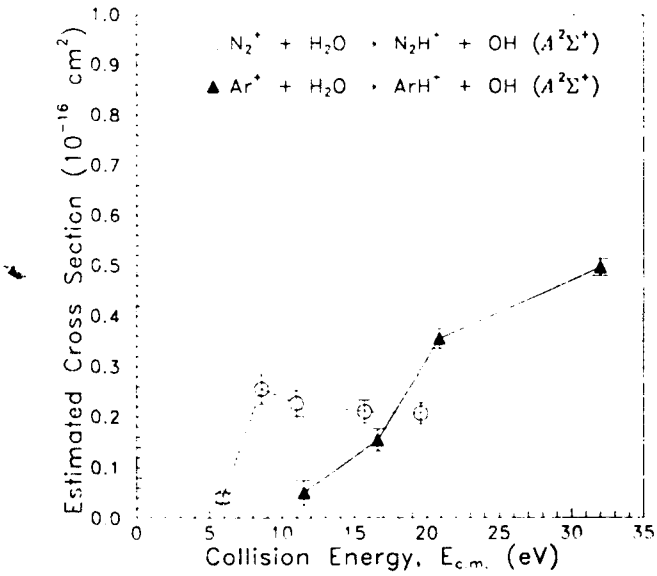

FIG. 12. Estimates for the OH A state formation cross section as a function of collision energy.

B. Reaction dynamics

Two rotational Boltzmann distributions are necessary to adequately simulate the emission data. This suggests that two channels are operative in forming excited OH, resulting in (i) excited and (ii) near-thermal rotational populations. As seen in Table I, the high T_{rot} case is the dominant channel. In this channel, A state OH is formed in both $v' = 0$ and $v' = 1$, with a collision energy-dependent T_{rot} that ranges from 1000 K at $E_{c.m.} = 6$ eV to 3400 K at $E_{c.m.} = 19$ eV. This channel is proposed to arise from a two-step reaction involving a long-range charge transfer, followed by a shorter range proton transfer to the "primary" species. Although little momentum is transferred in the large impact parameter charge-transfer collisions, it is still possible to reconcile the high OH rotational angular momentum with such collisions. In reactions (1) and (2), H_2O^+ is formed in highly excited bending vibrational levels of the linear $\tilde{A}$ state.[17] Following the loss of a proton, this H_2O^+ vibrational angular momentum most likely appears as OH rotational angular momentum. Similar correlations between H_2O ν_2 excitation and resulting OH rotational excitation has been reported by Sinha *et al.*[40] and by Bronikowski *et al.*[41] In those groups, specific vibrational modes of neutral H_2O (HDO) are laser excited. The vibrationally excited H_2O then undergoes hydrogen atom transfer (loss) reactions and the rotational population of the resulting OH is studied. In both cases, when the H_2O ν_2 (bending mode) is excited by even a small amount (e.g., to $v = 1$ or 2), the product OH is rotationally excited. In cases where both OH stretch local modes in the H_2O are excited, the final OH is also vibrationally excited. Similarly, the OH vibrational excitation observed here may indicate stretching excitation of the intermediate H_2O^+.

The other channel is characterized by formation of A state OH in the $v' = 0$ vibrational level with a rotational temperature profile matching $T_{rot} = 300$ K. Qualitatively, this rotational population is consistent with a pairwise interaction involving thermal H_2O that results in a direct hydrogen atom transfer. In such a mechanism, the primary ion would interact mainly with the hydrogen atom being stripped from the H_2O and the remaining OH would absorb enough energy to reach the A state. The vibrational distribution of thermal H_2O is essentially 100% in $v = 0$ (relative population of

$v = 1$ is $< 10^{-7}$ for the ν_1 and ν_3 stretching vibrations, and 5×10^{-4} for the ν_2 bending vibration). Removal of a hydrogen atom from such vibrationally relaxed H_2O is expected to produce rotationally cool OH.

Quantitatively, however, the predictions of the pairwise energy model differ from the observation of the OH A state threshold near 5 eV for reaction (3) and 12 eV for reaction (4). The pairwise energy model predicts that, for a reaction of the type $A + HB \rightarrow HA + B$, the translational collision energy available to internal modes of the products, E_{pair}, is given by[21]

$$E_{\text{pair}} = E_{\text{c.m.}} [(m_A + m_{HB}) m_H] / [m_{HA} m_{HB}].$$

For reaction (3), $E_{\text{pair}} = E_{\text{c.m.}} \times 0.088$, and for reaction (4), $E_{\text{pair}} = E_{\text{c.m.}} \times 0.079$. As mentioned earlier, production of A state OH is endothermic by 2.1 eV for reaction (3) and by 3.1 eV for reaction (4). The thresholds predicted for OH A state production, where E_{pair} equals the endothermicity, are therefore $E_{\text{c.m.}} = 24$ eV for reaction (3) and $E_{\text{c.m.}} = 39$ eV for reaction (4). A greater translational-to-internal energy transfer must occur for OH A state production than that predicted by the pairwise model below these thresholds. These reactions must therefore occur with relatively small impact parameters, presumably on repulsive surfaces that permit such transfer.[21] The transfer of the required energy would be reflected in a reduced kinetic-energy release. For example, at $E_{\text{c.m.}} = 11$ eV, the laboratory frame translational energy of N_2H^+ would be 1.1 eV lower than the pairwise energy prediction, which is $E_{HA} = E_A (m_A / m_{HA})$. The OH A state formation is therefore only possible in the low-energy tail of the observed N_2H^+ laboratory energy distributions.[2]

V. SUMMARY

The OH $A \rightarrow X$ emissions resulting from hydrogen atom pickup channels in $N_2^+ + H_2O$ and $Ar^+ + H_2O$ collisions at suprathermal energies are reported. Above a threshold of $E_{\text{c.m.}} \approx 5$ eV for $N_2^+ + H_2O$, the production of A state OH is found to account for less than 10% of the hydrogen atom pickup channel cross section and less than 1% of the total reaction cross section. For $Ar^+ + H_2O$, A state OH may be formed in all of the hydrogen atom pickup reactions above $E_{\text{c.m.}} \approx 15$ eV, but represents less than 2% of the total reaction cross section. Simulations of the OH emissions show two components: one that results from vibrationally and rotationally hot OH, and one that results from vibrationally and rotationally thermal OH. It is suggested that the two dynamic channels are due to a nonadiabatic atom transfer via the H_2O^+ surface and to a direct transfer, respectively.

ACKNOWLEDGMENT

This work is supported by the Air Force Office of Scientific Research under Task 2303G2.

[1] B. H. Mahan, in *An Analysis of Direct Ion-Molecule Reactions*, in *Interactions Between Ions and Molecules*, edited by P. Ausloos (Plenum, New York, 1975), p. 75.
[2] R. A. Dressler, J. A. Gardner, R. H. Salter, F. J. Wodarczyk, and E. Murad, J. Chem. Phys. **92**, 1117 (1990).
[3] R. A. Dressler, J. A. Gardner, D. L. Cooke, and E. Murad, J. Geophys. Res. **96A**, 13 795 (1991).
[4] J. F. Paulson, F. Dale, and S. A. Studniarz, *Int. J. Mass Spectrom. Ion Phys.* **5**, 113 (1970).
[5] E. W. Kaiser, A. Crowe, and W. E. Falconer, J. Chem. Phys. **61**, 2720 (1974).
[6] J. A. Rutherford and D. A. Vroom, J. Chem. Phys. **64**, 3057 (1976).
[7] M. Heninger, S. Fenistein, G. Mauclaire, R. Marx, and E. Murad, J. Geophys. Res. **16**, 139 (1989).
[8] C. R. Lishawa, R. A. Dressler, J. A. Gardner, R. H. Salter, and E. Murad, J. Chem. Phys. **93**, 3196 (1990).
[9] J. A. Gardner, R. A. Dressler, R. H. Salter, and E. Murad, J. Chem. Phys. **93**, 7780 (1990).
[10] J. A. Gardner, R. A. Dressler, R. H. Salter, and E. Murad, Chem. Phys. Lett. **181**, 5 (1991).
[11] T. R. Govers, P. M. Guyon, T. Baer, K. Cole, H. Frölich, and M. Lavollée, Chem. Phys. **87**, 373 (1984).
[12] P. Archirel and B. Levy, Chem. Phys. **106**, 51 (1986).
[13] G. Parlant and E. A. Gislason, J. Chem. Phys. **86**, 6183 (1987).
[14] E. A. Gislason and G. Parlant, Comments At. Mol. Phys. **19**, 157 (1987).
[15] For an extensive review, see *State-Selected and State-to-State Ion-Molecule Reaction Dynamics*, Vol. 82 of *Advanced Chemical Physics Part II*, edited by M. Baer and C. Y. Ng (Wiley, New York, 1992).
[16] R. A. Dressler, J. A. Gardner, C. R. Lishawa, R. H. Salter, and E. Murad, J. Chem. Phys. **93**, 9189 (1990).
[17] R. A. Dressler, J. A. Gardner, R. H. Salter, and E. Murad, J. Chem. Phys. **96**, 1062 (1992).
[18] K. Lacmann and A. Henglein, Ber. Buns. Phys. Chem. **69**, 292 (1965); A. Henglein, Adv. Mass Spectrom. **3**, 331 (1966); A. Ding, K. Lacmann, and A. Henglein, Ber. Berl. Buns. Ges. **71**, 596 (1967).
[19] M. Baer, Mol. Phys. **35**, 1637 (1978).
[20] R. H. Schultz and P. B. Armentrout, J. Chem. Phys. **96**, 1036 (1992).
[21] J. L. Elkind and P. B. Armentrout, J. Chem. Phys. **84**, 4862 (1986).
[22] R. Derai, S. Fenistein, M. Gerard-Ain, T. R. Govers, R. Marx, G. Mauclaire, C. Z. Profous, and C. Sourisseau, Chem. Phys. **44**, 65 (1979).
[23] J. Glosik, B. Friedrich, and Z. Herman, Chem. Phys. **60**, 369 (1981).
[24] Ch. Ottinger, in *Gas Phase Ion Chemistry*, edited by M. T. Bowers (Academic, New York, 1984), Vol. 3, p. 250.
[25] J. J. Leventhal, in *Gas Phase Ion Chemistry*, Ref. 24, p. 309.
[26] S. G. Lias, J. E. Bartmess, J. F. Liebman, J. L. Holmes, R. D. Levin, and W. G. Mallard, J. Phys. Chem. Ref. Data **17**, Suppl. 1 (1988).
[27] J. A. Gardner, R. A. Dressler, R. H. Salter, and E. Murad, Geophysics Laboratory (AFSC) Technical Report, GL-TR-89-0345 (1989).
[28] R. K. Lengel and D. R. Crosley, J. Chem. Phys. **67**, 2085 (1977).
[29] R. K. Lengel and D. R. Crosley, J. Chem. Phys. **68**, 5309 (1978).
[30] G. H. Dieke and H. M. Crosswhite, J. Quant. Spectrosc. Radiat. Transfer **2**, 97 (1962).
[31] The normal convention of a single prime for the upper state and a double prime for the lower state is followed here.
[32] I. L. Chidsey and D. R. Crosley, J. Quant. Spectrosc. Radiat. Transfer **23**, 187 (1980).
[33] K. R. German, J. Chem. Phys. **63**, 5252 (1975).
[34] Ch. Ottinger and J. Simonis, Chem. Phys. **28**, 97 (1978).
[35] D. E. Heard, D. R. Crosley, J. B. Jeffries, G. P. Smith, and A. Hirano, J. Chem. Phys. **96**, 4366 (1992).
[36] I. Kusunoki and Ch. Ottinger, J. Chem. Phys. **71**, 4227 (1979).
[37] S. R. Langhoff, E. F. van Dishoeck, R. Wetmore, and A. Dalgarno, J. Chem. Phys. **77**, 1379 (1982).
[38] P. Erman and J. Brzozowski, Phys. Lett. A **46**, 79 (1973).
[39] R. A. Dressler, J. A. Gardner, R. H. Salter, and E. Murad (unpublished).
[40] A. Sinha, J. D. Thoemke, and F. F. Crim, J. Chem. Phys. **96**, 372 (1992), and references therein.
[41] M. J. Bronikowski, W. R. Simpson, B. Girard, and R. N. Zare, Conference on the Dynamics of Molecular Collisions, Lake George, N.Y., 1991 (unpublished).